

A kinetic model for rarefied flows of molecular gas with vibrational modes

Qi Li and Lei Wu[†]

Department of Mechanics and Aerospace Engineering, Southern University of Science and Technology, Shenzhen 518055, China

(Received xx; revised xx; accepted xx)

A kinetic model is proposed for rarefied flows of molecular gas with rotational and temperature-dependent vibrational degrees of freedom. The model reduces to the Boltzmann equation for monatomic gas when the energy exchange between the translational and internal modes is absent, thus the influence of intermolecular potential can be captured. Moreover, not only the transport coefficients but also their fundamental relaxation processes are recovered. The accuracy of our kinetic model is validated by the direct simulation Monte Carlo method in several rarefied gas flows, including the shock wave, Fourier flow, Couette flow, and the creep flow driven by Maxwell's demon. Then the kinetic model is adopted to investigate thermally-induced flows. By adjusting the viscosity index in the Boltzmann collision operator, we find that the intermolecular potential significantly influences the velocity and Knudsen force. Interestingly, in the transition flow regime, the Knudsen force exerting on a heated beam could reverse the direction when the viscosity index changes from 0.5 (hard-sphere gas) to 1 (Maxwell gas). This discovery is useful in the design of micro-electromechanical systems for microstructure actuation and gas sensing.

1. Introduction

The non-equilibrium dynamics of molecular (diatomic/polyatomic) gas is commonly encountered in aerospace engineering. For example, at a high Mach number, the air surrounding an aircraft decelerates and heats up rapidly after compression by shock waves, which causes strong energy conversion from the translational energy into the internal energy. The temperature may reach thousands of degrees Kelvin and thus leads to significant changes in the physical and chemical properties of the gas (Anderson 2019; Ivano & Gimelshein 1998). Under the assumption of thermodynamic equilibrium, the traditional Navier-Stokes-Fourier equations are used to predict the thermal environment and aerodynamic characteristics of the aircraft. And the influence of internal degrees of freedom (DoF) is taken into account by the variations of heat capacity and transport properties of molecular gas (Malik & Anderson 1991). On the other hand, when the thermodynamic nonequilibrium occurs, gases with different temperatures associated with various relaxation processes needs to be considered. And several sets of Navier-Stokes-type equations have been developed with multi-temperatures of different types of kinetic modes (Colonna et al. 2006; Bruno & Giovangigli 2011; Aoki et al. 2020).

Since the macroscopic models are obtained at small Knudsen number, they are only applicable in the near-continuum flow regime. However, the gas could be in highly thermal nonequilibrium in many realistic situations, such as the reentry of aircraft into the atmosphere, where the gas flow changes from the continuum to the free-molecular regimes. Therefore, the treatment based on gas kinetic theory is inevitable, as the molecular dynamics simulation is limited to small spatial and temporal domains. The fundamental equation in gas kinetic theory is the Boltzmann equation, but it is only rigorously established for monatomic gas. For the molecular gas, its internal DoF pose

[†] Email address for correspondence: wul@sustech.edu.cn

difficulties in the modelling of rarefied gas dynamics. The heuristic way to describe the molecular gas dynamics in all flow regimes is the [Wang-Chang & Uhlenbeck \(1951\)](#) (WCU) equation, which treats the internal DoF quantum mechanically and assigns each internal energy level an individual velocity distribution function. However, the complexity and excessive computational burden prevent the application of WCU equation.

The direct simulation Monte Carlo (DSMC) method ([Bird 1994](#)) is prevailing in simulating the rarefied gas dynamics ([Frezzotti 2007](#); [Pfeiffer et al. 2016](#); [Tantos et al. 2016](#)). Although it is proven that DSMC is equivalent to the Boltzmann equation for monatomic gas ([Wagner 1992](#)), there are two drawbacks when applied to molecular gas flows. First, the bulk viscosity and the thermal conductivities cannot be recovered simultaneously. The reason lies in its phenomenological collision model of [Borgnakke & Larsen \(1975\)](#), which realizes the correct exchange rate between the translational and internal energies to exactly recover the bulk viscosity ([Haas et al. 1994](#); [Gimelshein et al. 2002](#)). However, it cannot guarantee that the thermal conductivity, or its translational and internal components, is recovered at the same time ([Wu et al. 2020](#); [Li et al. 2021](#)). Second, DSMC is not well suited to the simulation of low-speed flows due to its intrinsic stochastic nature. For instance, it has been found that the computational cost increases as Ma^{-2} (Ma is the Mach number) when the flow speed is approaching zero ([Hadjiconstantinou et al. 2003](#)). However, due to the rapid development of microelectromechanical techniques, the rarefied molecular gas conditions also exist in the flows at the microscale for a broad range of industrial applications ([Karniadakis et al. 2005](#)). And the speed of these small scale flows are usually much lower than the thermal velocity of gas molecules, thus making the DSMC time-consuming and even intractable in some cases.

Alternatively, kinetic models are proposed to imitate as closely as possible the behaviour of the WCU equation, and multiscale deterministic methods are developed to solve those kinetic models. The Bhatnagar-Gross-Krook (BGK) type kinetic models, which replace the Boltzmann collision operator with a single relaxation approximation ([Bhatnagar et al. 1954](#)), are very popular. Notable success has been achieved by the BGK model in the modelling of the monatomic rarefied gas. However, the Prandtl number is incorrect in its standard model. To overcome this issue, the modified BGK models, such as the ellipsoidal-statistical BGK model ([Holway 1966](#)) and the Shakhov model ([Shakhov 1968a](#)) have been proposed. These kinetic models have been extended to polyatomic rarefied gas by introducing additional internal energy variables in the distribution function ([Morse 1964](#); [Rykov 1975](#); [Andries et al. 2000b](#); [Rahimi & Struchtrup 2016](#); [Wang et al. 2017](#); [Bernard et al. 2019](#); [Dauvois et al. 2020](#)), as well as the gas mixture of polyatomic molecules ([Klingenberg et al. 2018](#); [Pirner 2018](#)). Besides, the Fokker-Planck models have been proposed ([Gorji & Jenny 2013](#); [Mathiaud & Mieussens 2020](#)), which take advantage of the continuous distribution functions in terms of stochastic velocity processes to speed up the stochastic particle methods.

However, these models do not reduce to the Boltzmann equation for monatomic gases when the translational-internal energy exchange is absent. Therefore, these models cannot distinguish the influence of different intermolecular potentials. For example, the uncertainties caused by different intermolecular potentials has been demonstrated in calculation of thermal creep slip on diffuse walls ([Loyalka 1990](#)), the thermal creep and Poiseuille flows ([Sharipov & Bertoldo 2009](#); [Takata & Funagane 2011](#)), the viscous slip of the Couette flow ([Su et al. 2019a](#)). On the other hand, all these kinetic model equations concern only the transport coefficients, such as the thermal conductivity and bulk viscosity, while their fundamental relaxation processes are not captured, which are found to be important in rarefied molecular gas dynamics. For example, the relaxation rates of heat flux can significantly affect the creep flow driven by molecular velocity-dependent external force ([Li et al. 2021](#)). Therefore, it is necessary to tackle the two difficulties when building a gas kinetic model for molecules with rotational and vibrational DoF.

This rest of the paper is organized as follows. In §2, the transport coefficients and their intrinsic

relation to relaxation rates are discussed, and the kinetic model is built based on the relaxation time approximation to reflect those relaxations. In §3, the kinetic model is further developed to incorporate the Boltzmann collision operator to discern the influence of intermolecular potentials. In §4, the kinetic model is validated by DSMC in typical rarefied gas flows. Then, in §5, the kinetic model is applied to solve two-dimensional thermally induced microflow, and the influence of intermolecular potential on the thermal transpiration and the Knudsen force on micro-beam is investigated by varying the viscosity index. Finally, conclusions are presented in §6.

2. Properties of molecular gas and relaxation-time approximation

A fundamental requirement in constructing a kinetic model is that all the transport coefficients are consistent with those obtained from the Boltzmann equation for monatomic gas or the WCU equation for molecular gas. Due to the excitation of internal DoF in molecular gas, additional relaxation processes occur between different type of energies, which lead to new transport coefficients such as the bulk viscosity and internal thermal conductivity. The recovery of these new transport coefficients in kinetic model is crucial to accurately describe rarefied gas dynamics in many problems. For instances, the modelling of the shock wave requires correct bulk viscosity due to its high compressibility, while the modelling of thermal transpiration requires the recovery of translational thermal conductivity, rather than the total thermal conductivity (Mason 1963; Porodnov et al. 1978; Loyalka & Storvick 1979). Therefore, in the following discussion, the transport coefficients, especially their intrinsic relaxation processes exclusively exist in molecular gas will be introduced, then the kinetic model will be established to recover these relaxation processes and transport coefficients.

2.1. Kinetic description of molecular gas

Both rotational and vibrational DoF of molecular gases are considered. In addition to the translational molecular velocity \mathbf{v} , the rotational energy I_r and vibrational energy I_v are introduced, and their corresponding numbers of DoF are d_r and d_v . It is noted that the translational and rotational DoF are fully activated at relatively low temperature; for example, for nitrogen when the temperature is higher than 10 K. Therefore, it is a common choice to use constant values of DoF for these modes. On the other hand, the vibrational DoF has not been significantly excited until 10^3 K. Therefore, the vibrational DoF depends on the vibrational temperature T_v :

$$d_v(T_v) = \frac{2T_{\text{ref}}/T_v}{\exp(T_{\text{ref}}/T_v) - 1}, \quad (2.1)$$

where T_{ref} is the characteristic temperature of the active vibrational mode.

Thus, the distribution function of gases is denoted as $f(t, \mathbf{x}, \mathbf{v}, I_r, I_v)$, where t is the time and \mathbf{x} is the spatial coordinates. Macroscopic variables, such as the number density n , flow velocity \mathbf{u} , heat fluxes $\mathbf{q}_t, \mathbf{q}_r, \mathbf{q}_v$, pressure tensor p_{ij} , and temperatures T_t, T_r, T_v , are obtained by taking the moments of the distribution function:

$$\begin{aligned} (n, \mathbf{nu}, p_{ij}) &= \int (1, \mathbf{v}, mc_i c_j) f d\mathbf{v} dI_r dI_v, \\ \left(\frac{3}{2} k_B T_t, \frac{d_r}{2} k_B T_r, \frac{d_v(T_v)}{2} k_B T_v \right) &= \frac{1}{n} \int \left(\frac{1}{2} mc^2, I_r, I_v \right) f d\mathbf{v} dI_r dI_v, \\ (\mathbf{q}_t, \mathbf{q}_r, \mathbf{q}_v) &= \int \mathbf{c} \left(\frac{1}{2} mc^2, I_r, I_v \right) f d\mathbf{v} dI_r dI_v, \end{aligned} \quad (2.2)$$

where the subscripts t, r, v indicate translational, rotational and vibrational components, respectively; $\mathbf{c} = \mathbf{v} - \mathbf{u}$ is the peculiar velocity, m is the molecular mass, and k_B is the Boltzmann constant.

We also define the temperature T_{tr} to be the equilibrium temperature between the translational and rotational modes, T_{tv} the equilibrium temperature between the translational and vibrational modes, and T the equilibrium temperature over all DoF:

$$T_{tr} = \frac{3T_t + d_r T_r}{3 + d_r}, \quad T_{tv} = \frac{3T_t + d_v(T_v)T_v}{3 + d_v(T_v)}, \quad T = \frac{3T_t + d_r T_r + d_v(T_v)T_v}{3 + d_r + d_v(T)}, \quad (2.3)$$

and the corresponding pressures are $[p_t, p_r, p_v, p, p_{tr}, p_{tv}] = nk_B [T_t, T_r, T_v, T, T_{tr}, T_{tv}]$.

2.2. Relaxation processes in molecular gas

In addition to the shear viscosity and translational heat conductivity in monatomic gas, the molecular gas possesses the bulk viscosity and internal thermal conductivities. The essence of these new transport coefficients are the relaxation of internal temperature and heat fluxes. This subsection is dedicated to the derivation of bulk viscosity and internal thermal conductivities, solely based on the relaxation processes.

2.2.1. Bulk viscosity

During the contraction or expansion of gas, the work done by pressure is converted to the translational energy immediately. However, in molecular gas, the molecules exhibit internal relaxation that exchanges the translational and internal energies in a finite time, which gives rise to the resistance that opposites to the volume change. This is known as the bulk viscosity.

According to the Jeans-Landau-Teller equation, the rotational and vibrational relaxation at macroscopic level can be described as,

$$\frac{DT_r}{Dt} = \frac{T_t - T_r}{\tau_r}, \quad \frac{DT_v}{Dt} = \frac{T_t - T_v}{\tau_v}, \quad (2.4)$$

where $D/Dt = \partial/\partial t + \mathbf{u} \cdot \partial/\partial \mathbf{x}$ is the material derivative, τ_r and τ_v are the relaxation time between the translational-rotational and translational-vibrational energy exchanges, respectively. Based on (2.3) and (2.4), the temperature change due to the effect of the relaxation alters T to T_t as follows:

$$T_t - T = \frac{1}{3 + d_r + d_v(T_v)} \left(d_r \frac{DT_r}{Dt} + d_v(T_v) \frac{DT_v}{Dt} \right). \quad (2.5)$$

Considering the relaxation time τ_r and τ_v are much smaller than the timescale of gas volume change, where the deviation between equilibrium temperature T and T_t , T_r , T_v are small, the higher order terms of $T - T_r$ and $T - T_v$ can be ignored. Then, we have,

$$T_t - T = \frac{d_r \tau_r + d_v(T_v) \tau_v}{3 + d_r + d_v(T_v)} \frac{DT}{Dt}. \quad (2.6)$$

Ignoring the effect of shear viscosity and heat conduction, the energy conservation follows,

$$p_t \nabla \cdot \mathbf{u} + \frac{3 + d_r + d_v(T_v)}{2} nk_B \frac{DT}{Dt} = 0. \quad (2.7)$$

Then, the pressure change due to the effect of the relaxation can be obtained by combining (2.6) and (2.7),

$$p = p_t + 2p_t \frac{d_r \tau_r + d_v(T_v) \tau_v}{[3 + d_r + d_v(T_v)]^2} \nabla \cdot \mathbf{u}. \quad (2.8)$$

Thus, the bulk viscosity is obtained as

$$\mu_b = 2p_t \frac{d_r \tau_r + d_v(T_v) \tau_v}{[3 + d_r + d_v(T_v)]^2}. \quad (2.9)$$

It is shown that when the numbers of DoF are fixed, the bulk viscosity is determined by the translational pressure and relaxation times of internal modes.

2.2.2. Thermal conductivity

The rotational and vibrational modes in molecular gas carry the thermal energy and contribute also to the heat flux, while the conductance can be quite different from that of the translational one. In the continuum flow limit, the total thermal conductivity can determine the gas dynamics in addition to the viscosity and diffusivity. However, the thermal conductivity of a single type mode may be important and even dominated when the gas is rarefied. For example, the mass flow rate in thermal transpiration is found to depend on the translational thermal conductivity of gas rather than the total thermal conductivity (Mason 1963).

In generally, the relaxation of translational and internal heat fluxes, q_t and q_{int} , satisfies the following relation in spatially-homogeneous system (Mason & Monchick 1962):

$$\begin{bmatrix} \partial \mathbf{q}_t / \partial t \\ \partial \mathbf{q}_{int} / \partial t \end{bmatrix} = -\frac{p_t}{\mu} \begin{bmatrix} A_{tt} & A_{ti} \\ A_{it} & A_{ii} \end{bmatrix} \begin{bmatrix} \mathbf{q}_t \\ \mathbf{q}_{int} \end{bmatrix}, \quad (2.10)$$

where μ is the shear viscosity, the matrix \mathbf{A} encapsulates the dimensionless thermal relaxation rates, and the subscripts i represent the internal mode. From the Chapman-Enskog expansion, the thermal relaxation rates are related to the translational and internal thermal conductivities, κ_t and κ_{int} , respectively, as

$$\begin{bmatrix} \kappa_t \\ \kappa_{int} \end{bmatrix} = \frac{k_B \mu}{2m} \begin{bmatrix} A_{tt} & A_{ti} \\ A_{it} & A_{ii} \end{bmatrix}^{-1} \begin{bmatrix} 5 \\ d_{int} \end{bmatrix}, \quad (2.11)$$

where d_{int} is the number of all internal DoF.

It will be convenient to use the following dimensionless Eucken (1913) factor f_{eu} :

$$c_v f_{eu} \equiv \frac{\kappa}{\mu} = \frac{\kappa_t + \kappa_{int}}{\mu}, \quad (2.12)$$

where κ is the total thermal conductivity, and c_v is the specific heat capacity at constant volume. Similarly, f_t and f_{int} represent the Eucken factors of the translational and internal modes, respectively,

$$f_t = \frac{2}{3} \frac{m \kappa_t}{k_B \mu}, \quad f_{int} = \frac{2}{d_{int}} \frac{m \kappa_r}{k_B \mu}. \quad (2.13)$$

The total Eucken factor f_{eu} can be determined directly from the total thermal conductivity, which can be measured experimentally. However, those of the translational and internal parts are rather difficult to be obtained. Nevertheless, Mason & Monchick (1962) derived the approximate thermal relaxation rates \mathbf{A} ,

$$A_{tt} = \frac{2}{3} + \frac{5d_{int}\tau}{18\tau_{int}}, \quad A_{ii} = \frac{\mu}{\rho D'} + \frac{3\tau}{6\tau_{int}}, \quad A_{ti} = -\frac{5\tau}{6\tau_{int}}, \quad A_{it} = -\frac{d_{int}\tau}{6\tau_{int}}, \quad (2.14)$$

where $\rho = nm$ is the mass density, τ is the relaxation time of translational modes to reach equilibrium, τ_{int} is the relaxation time of translational-internal energy exchange and D' is the average diffusion coefficient. Therefore, the translational and internal Eucken factors are determined,

$$f_t = \frac{5}{2} \left[1 - \frac{5d_{int}\tau}{12\tau_{int}} \left(1 - \frac{2\rho D'}{5\mu} \right) \right], \quad f_{int} = \frac{\rho D'}{\mu} \left[1 + \frac{5\tau}{4\tau_{int}} \left(1 - \frac{2\rho D'}{5\mu} \right) \right]. \quad (2.15)$$

To match the experimental values of thermal conductivity, the internal relaxation time τ_{int} in the above equations has to be modified (Mason & Monchick 1962). However, from (2.9) it follows that the internal relaxation time determines the bulk viscosity, which means that the bulk viscosity and all thermal conductivities cannot be recovered simultaneously, if (2.15) is used. To get rid of this problem, exact values of thermal relaxation rates \mathbf{A} should be incorporated into the kinetic model.

2.3. Kinetic model with relaxation time approximation

It is well known that the evolution of the molecular gas distribution function is governed by the Wang-Chang & Uhlenbeck (1951) equation, which is too complicated to be applied in realistic problems. Therefore, kinetic models are urgently needed to simplify the collision operator in the WCU equation. Well-known kinetic models are the stochastic Borgnakke & Larsen (1975) model and the deterministic Rykov (1975) and ellipsoidal-statistical BGK models (Holway Jr 1966; Andries et al. 2000a), with the emphasis to recover the transport coefficients, rather than the essential relaxation process (2.11). To be specific, in both deterministic kinetic models, the cross-relaxation coefficients A_{ti} and A_{it} vanish. As a consequence, the ellipsoidal-statistical BGK model cannot recover f_{ir} and f_{int} , although the total Eucken factor is correct; the Rykov model can recover f_{ir} and f_{int} , and therefore has flexibility in the simulation of thermal transpiration, but in the rarefied flow driven by the Maxwell demon the velocity is incorrect (Li et al. 2021).

We now try to build a kinetic model based on the Rykov model, due to its more freedom to reflect the relaxation process of heat fluxes. In this model, the elastic and inelastic collisions are considered separately with different relaxation time, which can be adjusted to give a correct bulk viscosity. And the reference distribution functions to which the distribution function relaxes contain the heat fluxes, so that the thermal conductivity can be recovered. Although the Rykov model is initially proposed for diatomic gas without vibrational modes, it has been extended to polyatomic gas (Wu et al. 2015b) and gases with vibrational modes (Titarev & Frolova 2018). By adjusting the heat fluxes in the reference distribution functions, (2.11) can be properly recovered.

For inelastic collisions, only the relaxation processes between translational-rotational and translational-vibrational DoF are considered, due to the weak rotational-vibrational relaxation. Thus, the evolution of the distribution function $f(\mathbf{x}, \mathbf{v}, I_r, I_v, t)$ under external body acceleration \mathbf{a} is governed by

$$\frac{\partial f}{\partial t} + \mathbf{v} \cdot \frac{\partial f}{\partial \mathbf{x}} + \frac{\partial(\mathbf{a}f)}{\partial \mathbf{v}} = \underbrace{\frac{g_t - f}{\tau}}_{elastic} + \underbrace{\frac{g_r - g_t}{Z_r \tau} + \frac{g_v - g_t}{Z_v \tau}}_{inelastic} \quad (2.16)$$

where Z_r and Z_v are the rotational and vibrational collision number, respectively. Since the acceleration \mathbf{a} could be velocity dependent under general consideration, it is kept inside the partial derivative with respect to \mathbf{v} . The reference distribution functions g_t, g_r, g_v are expanded about the equilibrium distributions $E_t(T) \cdot E_r(T) \cdot E_v(T)$ in a series of orthogonal polynomials in variables peculiar velocity \mathbf{c} , rotational energy I_r , vibrational energy I_v and corresponding moments $\mathbf{q}_t, \mathbf{q}_r, \mathbf{q}_v$:

$$\left. \begin{aligned} g_t &= E_t(T_t) \cdot E_r(T_r) \cdot E_v(T_v) \cdot \left[1 + \frac{2m\mathbf{q}_t \cdot \mathbf{c}}{15k_B T_t p_t} \left(\frac{mc^2}{2k_B T_t} - \frac{5}{2} \right) \right. \\ &\quad \left. + \frac{2m\mathbf{q}_r \cdot \mathbf{c}}{d_r k_B T_t p_r} \left(\frac{I_r}{k_B T_r} - \frac{d_r}{2} \right) + \frac{2m\mathbf{q}_v \cdot \mathbf{c}}{d_v(T_v) k_B T_t p_v} \left(\frac{I_v}{k_B T_v} - \frac{d_v(T_v)}{2} \right) \right], \\ g_r &= E_t(T_{tr}) \cdot E_r(T_{tr}) \cdot E_v(T_v) \cdot \left[1 + \frac{2m\mathbf{q}_0 \cdot \mathbf{c}}{15k_B T_{tr} p_{tr}} \left(\frac{mc^2}{2k_B T_{tr}} - \frac{5}{2} \right) \right. \\ &\quad \left. + \frac{2m\mathbf{q}_1 \cdot \mathbf{c}}{d_r k_B T_{tr} p_{tr}} \left(\frac{I_r}{k_B T_{tr}} - \frac{d_r}{2} \right) + \frac{2m\mathbf{q}_2 \cdot \mathbf{c}}{d_v(T_v) k_B T_{tr} p_v} \left(\frac{I_v}{k_B T_v} - \frac{d_v(T_v)}{2} \right) \right], \\ g_v &= E_t(T_{tv}) \cdot E_r(T_r) \cdot E_v(T_{tv}) \cdot \left[1 + \frac{2m\mathbf{q}_0 \cdot \mathbf{c}}{15k_B T_{tv} p_{tv}} \left(\frac{mc^2}{2k_B T_{tv}} - \frac{5}{2} \right) \right. \\ &\quad \left. + \frac{2m\mathbf{q}_1 \cdot \mathbf{c}}{d_r k_B T_{tv} p_r} \left(\frac{I_r}{k_B T_r} - \frac{d_r}{2} \right) + \frac{2m\mathbf{q}_2 \cdot \mathbf{c}}{d_v(T_{tv}) k_B T_{tv} p_{tv}} \left(\frac{I_v}{k_B T_{tv}} - \frac{d_v(T_{tv})}{2} \right) \right], \end{aligned} \right\} \quad (2.17)$$

with the equilibrium distribution functions,

$$\left. \begin{aligned} E_t(T) &= n \left(\frac{m}{2\pi k_B T} \right)^{3/2} \exp \left(-\frac{mc^2}{2k_B T} \right), \\ E_r(T) &= \frac{I_r^{d_r/2-1}}{\Gamma(d_r/2)(k_B T)^{d_r/2}} \exp \left(-\frac{I_r}{k_B T} \right), \\ E_v(T) &= \frac{I_v^{d_v(T)/2-1}}{\Gamma(d_v(T)/2)(k_B T)^{d_v/2}} \exp \left(-\frac{I_v}{k_B T} \right). \end{aligned} \right\} \quad (2.18)$$

where Γ is the gamma function, \mathbf{q}_0 , \mathbf{q}_1 , and \mathbf{q}_2 are linear combinations of translational, rotational and vibrational heat fluxes.

2.4. Determination of model parameters

So far, the kinetic model equation (2.16) with the reference distributions in (2.17) contain the free parameters \mathbf{q}_0 , \mathbf{q}_1 , \mathbf{q}_2 , Z_r , Z_v , and τ . They will be determined by the recovery of relaxation rates of shear stress, temperature, and heat fluxes, which corresponding to the recover of shear viscosity, bulk viscosity, and thermal conductivities, respectively.

2.4.1. Relaxation of temperature

For simplicity let us consider a spatial-homogeneous system without the external acceleration. Multiply the equation (2.16) by $\frac{1}{2}mc^2$, I_r , I_v , and integrate them with respect to ν , I_r and I_v , yielding

$$\begin{aligned} \frac{\partial T_t}{\partial t} &= \frac{T_{tr} - T_t}{Z_r \tau} + \frac{T_{tv} - T_t}{Z_v \tau}, \\ \frac{\partial T_r}{\partial t} &= \frac{T_{tr} - T_r}{Z_r \tau}, \\ \frac{\partial (d_v(T_v)T_v)}{\partial t} &= \frac{d_v(T_{tv})T_{tv} - d_v(T_v)T_v}{Z_v \tau}. \end{aligned} \quad (2.19)$$

Comparing to the Jeans–Landau–Teller equations (2.4), the collision numbers relate to the relaxation time τ_r and τ_v are

$$Z_r = \frac{3\tau_r}{(3 + d_r)\tau}, \quad Z_v = \frac{3\tau_v}{(3 + d_v)\tau}. \quad (2.20)$$

Based on number density conservation and the definition of equilibrium temperature in equations (2.3), the conservation of total energy is guaranteed.

2.4.2. Relaxation of heat flux

In the original Rykov model, the relaxation of translational heat flux is independent of the rotational one, and vice versa. However, due to the energy exchange between different modes, it is necessary to consider the fact that the relaxations of heat fluxes are coupled within all the DoF. Thus, in analogy to (2.10), the relaxation of translational, rotational and vibrational heat fluxes are generalized to

$$\begin{bmatrix} \partial \mathbf{q}_t / \partial t \\ \partial \mathbf{q}_r / \partial t \\ \partial \mathbf{q}_v / \partial t \end{bmatrix} = -\frac{p_t}{\mu} \begin{bmatrix} A_{tt} & A_{tr} & A_{tv} \\ A_{rt} & A_{rr} & A_{rv} \\ A_{vt} & A_{vr} & A_{vv} \end{bmatrix} \begin{bmatrix} \mathbf{q}_t \\ \mathbf{q}_r \\ \mathbf{q}_v \end{bmatrix}, \quad (2.21)$$

where the dimensionless relaxation rates \mathbf{A} is a 3×3 matrix including all three types of modes. Accordingly, \mathbf{q}_0 , \mathbf{q}_1 , \mathbf{q}_2 in reference distributions (2.17) can be determined in terms of \mathbf{q}_t , \mathbf{q}_r , \mathbf{q}_v

and the thermal relaxation rates \mathbf{A} . To be specific, the governing equation (2.16) is multiplied by $\frac{1}{2}mc^2\mathbf{c}$, $I_r\mathbf{c}$ and $I_v\mathbf{c}$, respectively, and then are integrated with respect to \mathbf{v} , I_r and I_v , yielding

$$\begin{bmatrix} \mathbf{q}_0 \\ \mathbf{q}_1 \\ \mathbf{q}_2 \end{bmatrix} = \begin{bmatrix} (2 - 3A_{tt})Z_{int} + 1 & -3A_{tr}Z_{int} & -3A_{tv}Z_{int} \\ -A_{rt}Z_{int} & -A_{rr}Z_{int} + 1 & -A_{rv}Z_{int} \\ -A_{vt}Z_{int} & -A_{vr}Z_{int} & -A_{vv}Z_{int} + 1 \end{bmatrix} \begin{bmatrix} \mathbf{q}_t \\ \mathbf{q}_r \\ \mathbf{q}_v \end{bmatrix}, \quad (2.22)$$

where $Z_{int} = (1/Z_r + 1/Z_v)^{-1}$.

2.4.3. Shear viscosity and bulk viscosity

As it is discussed above, other than the shear viscosity, the bulk viscosity arises from the resistance of contraction or expansion in molecular gas, due to the energy exchange between translational and internal motions. And both of them can be derived based on the Chapman-Enskog expansion (Chapman & Cowling 1970), when the system is close to equilibrium. To the second approximation of the distribution, it is assumed $f = f^{(0)} + f^{(1)}$, where $f^{(0)} = E_t(T)E_r(T)E_v(T)$ is the equilibrium distribution at temperature T . Let $\mathcal{D}f \equiv \partial f/\partial t + \mathbf{v} \cdot \partial f/\partial \mathbf{x} + \mathbf{a} \cdot \partial f/\partial \mathbf{v}$, and consider $\mathcal{D}^{(0)}f = 0$, according to Chapman-Enskog expansion and the governing equation (2.16), we have

$$f^{(1)} = g_t - f^{(0)} + \frac{1}{Z_r}(g_r - g_t) + \frac{1}{Z_v}(g_v - g_t) - \tau \mathcal{D}^{(1)}f, \quad (2.23)$$

where

$$\begin{aligned} \mathcal{D}^{(1)}f &= \frac{\partial f^{(0)}}{\partial t} + \mathbf{v} \cdot \frac{\partial f^{(0)}}{\partial \mathbf{x}} + \mathbf{a} \cdot \frac{\partial f^{(0)}}{\partial \mathbf{v}} \\ &= f^{(0)} \left[\left(\left(\frac{mc^2}{2k_B T} - \frac{5}{2} \right) + \left(\frac{I_r}{k_B T} - \frac{d_r}{2} \right) + \left(\frac{I_v}{k_B T} - \frac{d_v}{2} \right) \right) \mathbf{c} \cdot \nabla \ln T \right. \\ &\quad \left. + \frac{2}{(3 + d_r + d_v)} \left(\frac{d_r + d_v}{3} \left(\frac{mc^2}{2k_B T} - \frac{3}{2} \right) - \left(\frac{I_r}{k_B T} - \frac{d_r}{2} \right) - \left(\frac{I_v}{k_B T} - \frac{d_v}{2} \right) \right) \frac{\partial u_i}{\partial x_i} \right. \\ &\quad \left. + \frac{m}{k_B T} c_{<i}c_{j>} \frac{\partial u_i}{\partial x_j} \right], \end{aligned} \quad (2.24)$$

$c_{<i}c_{j>} = c_i c_j - c^2 \delta_{ij}$, and δ_{ij} is the Kronecker delta function.

The pressure tensor p_{ij} is calculated as

$$\begin{aligned} p_{ij} &= \int mc_i c_j (f^{(0)} + f^{(1)}) d\mathbf{v} dI_r dI_v \\ &= \left(p_t + \frac{1}{Z_r}(p_{tr} - p_t) + \frac{1}{Z_v}(p_{tv} - p_t) \right) \delta_{ij} - p\tau \frac{\partial u_{<i}}{\partial x_{j>}} - p\tau \frac{2(d_r + d_v)}{3(3 + d_r + d_v)} \frac{\partial u_k}{\partial x_k} \delta_{ij} \\ &= p\delta_{ij} - p\tau \frac{\partial u_{<i}}{\partial x_{j>}} - 2p\tau \frac{(3 + d_r)d_r Z_r + (3 + d_v)d_v Z_v}{3(3 + d_r + d_v)^2} \frac{\partial u_i}{\partial x_i} \delta_{ij}, \end{aligned} \quad (2.25)$$

where $\partial u_{<i}/\partial x_{j>} = \partial u_i/\partial x_j + \partial u_j/\partial x_i - \frac{2}{3}(\partial u_k/\partial x_k)\delta_{ij}$. The shear viscosity μ and bulk viscosity μ_b are then obtained:

$$\begin{aligned} \mu(T_t) &= p_t \tau, \\ \mu_b(T_t) &= 2p_t \tau \frac{(3 + d_r)d_r Z_r + (3 + d_v)d_v Z_v}{3(3 + d_r + d_v)^2}. \end{aligned} \quad (2.26)$$

Therefore, it is shown that the ratio μ_b/μ depends only on the numbers of internal DoF and corresponding collision numbers. Larger Z_r or Z_v makes the energy exchange between translational and internal motions more difficult, thus lead to higher bulk viscosity.

2.4.4. Thermal conductivity and Eucken factors

Consider a homogeneous system of molecular gas at rest, where the spatial derivatives of flow velocity vanish in (2.24), the translational, rotational and vibrational heat fluxes can be calculated based on (2.2) and (2.21). Eventually we have

$$\begin{aligned} \begin{bmatrix} \mathbf{q}_t \\ \mathbf{q}_r \\ \mathbf{q}_v \end{bmatrix} &= \int \mathbf{c} \begin{bmatrix} \frac{1}{2}mc^2 \\ I_r \\ I_v \end{bmatrix} \left(f^{(0)} + f^{(1)} \right) d\mathbf{v} dI_r dI_v \\ &= \tau \begin{bmatrix} \partial \mathbf{q}_t / \partial t \\ \partial \mathbf{q}_r / \partial t \\ \partial \mathbf{q}_v / \partial t \end{bmatrix} + \begin{bmatrix} \mathbf{q}_t \\ \mathbf{q}_r \\ \mathbf{q}_v \end{bmatrix} - \frac{k_B \mu}{2m} \begin{bmatrix} 5 \\ d_r \\ d_v(T_v) \end{bmatrix} \nabla T. \end{aligned} \quad (2.27)$$

Consider $(\mathbf{q}_t, \mathbf{q}_r, \mathbf{q}_v) = -(\kappa_t, \kappa_r, \kappa_v) \nabla T$, then the thermal conductivities are

$$\begin{bmatrix} \kappa_t \\ \kappa_r \\ \kappa_v \end{bmatrix} = \frac{k_B \mu}{2m} \begin{bmatrix} A_{tt} & A_{tr} & A_{tv} \\ A_{rt} & A_{rr} & A_{rv} \\ A_{vt} & A_{vr} & A_{vv} \end{bmatrix}^{-1} \begin{bmatrix} 5 \\ d_r \\ d_v(T_v) \end{bmatrix}, \quad (2.28)$$

And the dimensionless parameters Eucken factors are calculated based on (2.13):

$$\begin{bmatrix} f_t \\ f_r \\ f_v \end{bmatrix} = \begin{bmatrix} 3A_{tt} & d_r A_{tr} & d_v(T_v) A_{tv} \\ 3A_{rt} & d_r A_{rr} & d_v(T_v) A_{rv} \\ 3A_{vt} & d_r A_{vr} & d_v(T_v) A_{vv} \end{bmatrix}^{-1} \begin{bmatrix} 5 \\ d_r \\ d_v(T_v) \end{bmatrix}. \quad (2.29)$$

Clearly, the elements in matrix \mathbf{A} cannot be fully determined even though all the Eucken factors f_t, f_r, f_v (thermal conductivities $\kappa_t, \kappa_r, \kappa_v$ equivalently) are fixed. In other words, in molecular gas, having all the transport coefficients is not enough to exactly describe the relaxation of heat flux, which may lead to uncertainty in predicting macroscopic gas dynamics (Li et al. 2021). Therefore, it is necessary to reconfirm the thermal relaxation rates in the kinetic model correctly.

3. Kinetic model with Boltzmann collision operator

In practical numerical simulations, it is better to eliminate the internal energy variables I_r, I_v , by introducing the following reduced velocity distribution functions f_0, f_1, f_2 :

$$(f_0, f_1, f_2) = \iint_0^\infty (1, I_r, I_v) f(t, \mathbf{x}, \mathbf{v}, I_r, I_v) dI_r dI_v. \quad (3.1)$$

Then, the governing equation (2.16) can be transferred to three coupled equations:

$$\frac{\partial f_l}{\partial t} + \mathbf{v} \cdot \frac{\partial f_l}{\partial \mathbf{x}} + \frac{\partial(\mathbf{a} f_l)}{\partial \mathbf{v}} = \frac{g_{lt} - f_l}{\tau} + \frac{g_{lr} - g_{lt}}{Z_r \tau} + \frac{g_{lv} - g_{lt}}{Z_v \tau}, \quad l = 0, 1, 2, \quad (3.2)$$

where the reduced reference velocity distribution functions are

$$\begin{aligned} g_{0t} &= E_t(T_t) \left[1 + \frac{2m\mathbf{q}_t \cdot \mathbf{c}}{15k_B T_t p_t} \left(\frac{mc^2}{2k_B T_t} - \frac{5}{2} \right) \right], \\ g_{0r} &= E_t(T_{tr}) \left[1 + \frac{2m\mathbf{q}_0 \cdot \mathbf{c}}{15k_B T_{tr} p_{tr}} \left(\frac{mc^2}{2k_B T_{tr}} - \frac{5}{2} \right) \right], \\ g_{0v} &= E_t(T_{tv}) \left[1 + \frac{2m\mathbf{q}_0 \cdot \mathbf{c}}{15k_B T_{tv} p_{tv}} \left(\frac{mc^2}{2k_B T_{tv}} - \frac{5}{2} \right) \right], \end{aligned} \quad (3.3)$$

and

$$\begin{aligned}
g_{1t} &= \frac{d_r}{2} k_B T_r g_{0t} + \frac{m \mathbf{q}_r \cdot \mathbf{c}}{p_t} E_t(T_t), \\
g_{1r} &= \frac{d_r}{2} k_B T_{tr} g_{0r} + \frac{m \mathbf{q}_1 \cdot \mathbf{c}}{p_{tr}} E_t(T_{tr}), \\
g_{1v} &= \frac{d_r}{2} k_B T_r g_{0v} + \frac{m \mathbf{q}_1 \cdot \mathbf{c}}{p_{tv}} E_t(T_{tv}), \\
g_{2t} &= \frac{d_v(T_v)}{2} k_B T_v g_{0t} + \frac{m \mathbf{q}_v \cdot \mathbf{c}}{p_t} E_t(T_t), \\
g_{2r} &= \frac{d_v(T_v)}{2} k_B T_v g_{0r} + \frac{m \mathbf{q}_2 \cdot \mathbf{c}}{p_{tr}} E_t(T_{tr}), \\
g_{2v} &= \frac{d_v(T_{tv})}{2} k_B T_{tv} g_{0v} + \frac{m \mathbf{q}_2 \cdot \mathbf{c}}{p_{tv}} E_t(T_{tv}).
\end{aligned} \tag{3.4}$$

The macroscopic quantities defined in (2.2) can be calculated based on the reduced velocity distribution functions:

$$\begin{aligned}
(n, n\mathbf{u}, p_{ij}) &= \int (1, \mathbf{v}, mc_i c_j) f_0 d\mathbf{v}, \\
\left(\frac{3}{2} k_B T_t, \frac{d_r}{2} k_B T_r, \frac{d_v(T_v)}{2} k_B T_v \right) &= \frac{1}{n} \int \left(\frac{1}{2} mc^2 f_0, f_1, f_2 \right) d\mathbf{v}, \\
(\mathbf{q}_t, \mathbf{q}_r, \mathbf{q}_v) &= \int \mathbf{c} \left(\frac{1}{2} mc^2 f_0, f_1, f_2 \right) d\mathbf{v}.
\end{aligned} \tag{3.5}$$

It is noted that although the kinetic model (2.16) is proposed as per classical mechanics, i.e., the vibrational energy levels are continuous. From the perspective of quantum mechanics, the discrete levels of vibrational energy need to be involved (Anderson 2019), and this large number of DoF due to the internal modes makes the trace of distribution function time-consuming. Fortunately, this is not necessary since the fundamental task is to obtain the evolution of macroscopic measurable quantities. It is shown that the complexity arising from the discrete vibrational energy can be eliminated with the reduced distribution technique (Mathiaud & Mieussens 2020). Therefore, by summation over all vibrational DoF and energy levels, the kinetic model proposed in this work is not restricted by the classical mechanics treatment of internal DoF.

Obviously, all molecules relax with the same speed in the relaxation-time approximation (2.16), which is not very physical, since in general molecules with larger peculiar velocity has larger collision probability and hence smaller relaxation time; in fact, when (2.16) is used, the temperature of normal shock wave will be overpredicted (Wu et al. 2015b). To circumvent this problem, by observing that the elastic collision term in (3.2) with $l = 0$ is just the Shakhov-type approximation of the Boltzmann collision operator for monatomic gas (Shakhov 1968a,b), we replace the elastic collision term $(g_{0t} - f_0)/\tau$ with the Boltzmann collision operator $Q(f_0)$ in monatomic gas:

$$Q(f_0) = \int_{\mathbb{R}^3} \int_{\mathbb{S}^2} B(\cos \theta, |\mathbf{v} - \mathbf{v}_*|) [f_0(\mathbf{v}'_*) f_0(\mathbf{v}') - f_0(\mathbf{v}_*) f_0(\mathbf{v})] d\Omega d\mathbf{v}_*, \tag{3.6}$$

so that the relaxation time depends on the molecular velocity. Meanwhile, g_{1t} and g_{2t} are modified

correspondingly (Wu et al. 2015b), resulting in the following kinetic model for molecular gas:

$$\begin{aligned}\frac{\partial f_0}{\partial t} + \mathbf{v} \cdot \frac{\partial f_0}{\partial \mathbf{x}} + \frac{\partial(\mathbf{a}f_0)}{\partial \mathbf{v}} &= Q(f_0) + \frac{g_{0r} - g_{0t}}{Z_r \tau} + \frac{g_{0v} - g_{0t}}{Z_v \tau}, \\ \frac{\partial f_1}{\partial t} + \mathbf{v} \cdot \frac{\partial f_1}{\partial \mathbf{x}} + \frac{\partial(\mathbf{a}f_1)}{\partial \mathbf{v}} &= \frac{g'_{1t} - f_1}{\tau} + \frac{g_{1r} - g_{1t}}{Z_r \tau} + \frac{g_{1v} - g_{1t}}{Z_v \tau}, \\ \frac{\partial f_2}{\partial t} + \mathbf{v} \cdot \frac{\partial f_2}{\partial \mathbf{x}} + \frac{\partial(\mathbf{a}f_2)}{\partial \mathbf{v}} &= \frac{g'_{2t} - f_2}{\tau} + \frac{g_{2r} - g_{2t}}{Z_r \tau} + \frac{g_{2v} - g_{2t}}{Z_v \tau},\end{aligned}\quad (3.7)$$

with

$$\begin{aligned}g'_{1t} &= \frac{d_r}{2} k_B T_r [\tau Q(f_0) + f_0] + \frac{m \mathbf{q}_r \cdot \mathbf{c}}{p_t} E_t(T_t), \\ g'_{2t} &= \frac{d_v(T_v)}{2} k_B T_v [\tau Q(f_0) + f_0] + \frac{m \mathbf{q}_v \cdot \mathbf{c}}{p_t} E_t(T_t).\end{aligned}\quad (3.8)$$

Since the Shakhov model and the Boltzmann equation have the same shear viscosity and translational thermal conductivity, it can be shown that the new model (3.7) has the same transport coefficients with the model (3.2).

Note that in (3.6), θ is the deflection angle of collision, \mathbf{v} and \mathbf{v}_* are the velocities of the two molecules before collision, while \mathbf{v}' and \mathbf{v}'_* are the velocities of the two molecules after collision, and Ω is the solid angle. $B(\cos \theta, |\mathbf{v} - \mathbf{v}_*|)$ is the collision kernel, which incorporates the role of intermolecular potential. When the inverse power-law potential is considered, the collision kernel is modelled as (Wu et al. 2013, 2014)

$$B = \frac{5\sqrt{\pi m k_B T_0} (4k_B T_0/m)^{(2\omega-1)/2}}{64\pi\mu(T_0)\Gamma^2(9/4 - \omega/2)} \sin^{(1-2\omega)/2} \left(\frac{\theta}{2} \right) \cos^{(1-2\omega)/2} \left(\frac{\theta}{2} \right) |\mathbf{v}_r|^2^{(1-\omega)}, \quad (3.9)$$

where ω is the viscosity index, that is,

$$\mu(T) = \mu(T_0) \left(\frac{T}{T_0} \right)^\omega. \quad (3.10)$$

Therefore, this kinetic model is able to distinguish the role of intermolecular potentials (Sharipov & Bertoldo 2009; Takata & Funagane 2011; Wu et al. 2014, 2015a), while the models based on the relaxation-time approximation do not have this capability.

4. Validation of the kinetic model

To evaluate the accuracy of the kinetic model (3.7), numerical solutions of one-dimensional Fourier flow, Couette flow, thermal creep flow and normal shock wave in nitrogen with constant vibrational DoF are compared with DSMC solutions. The kinetic model equations are solved by the discretized velocity method with the fast spectral method for the Boltzmann collision operator (Wu et al. 2013, 2014), while DSMC simulations are conducted using the open source code SPARTA (Plimpton et al. 2019).

In the following paper, dimensionless variables will be presented. The density, velocity, temperature, stress, and heat flux are normalized by the reference number density n_0 , the most probable speed $v_m = \sqrt{2k_B T_0/m}$, the reference temperature T_0 , $n_0 k_B T_0$, and $n_0 k_B T_0 v_m$, respectively. The spatial variable is normalized by the characteristic flow length L_0 , and the Knudsen number is defined as

$$\text{Kn} = \frac{\mu(T_0)}{n_0 L_0} \sqrt{\frac{\pi}{2m k_B T_0}}. \quad (4.1)$$

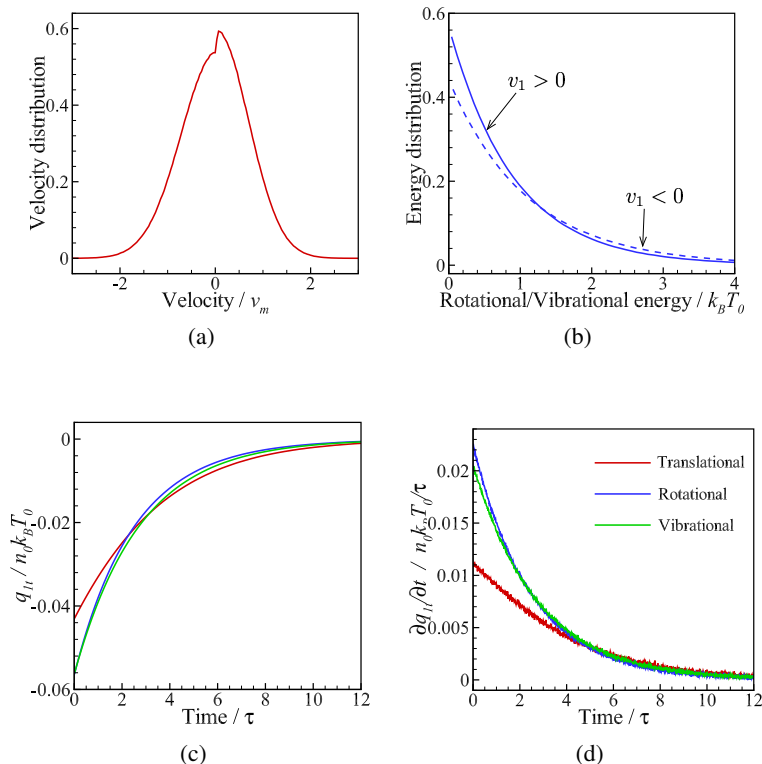


Figure 1: Extraction of the thermal relaxation rates A in (2.21) from the DSMC simulation. Special distributions of (a) the molecular velocity and (b) rotational/vibrational energy are designed to generate initial heat flux. (c) The evolution of heat fluxes and (d) their time derivatives are monitored until the system reaches thermal equilibrium.

4.1. Relaxation rates extracted from DSMC

Since the bulk viscosity and thermal conductivity cannot be adjusted independently in DSMC, we extract the thermal relaxation rates from the DSMC and apply to our kinetic model, to make a fair comparison. With the fixed shear viscosity and self-diffusion coefficient, the collision number Z_r and Z_v are the only parameters that affect the thermal relaxation rates in DSMC. Here we take $Z_r = 2.667$ and $Z_v = 10Z_r$.

Similar to the procedure of extracting thermal relaxation rates for the translational and rotational DoF from DSMC (Li et al. 2021), here a homogeneous system of nitrogen is simulated, which consists of 10^6 simulation particles in a cubic cell of the size $(10 \text{ nm})^3$. The periodic condition is applied at all boundaries. Binary collisions are described by the variable soft sphere model, and the system parameters and properties of nitrogen used in the simulations are: $d_r = d_v = 2$, $n_0 = 2.69 \times 10^{25} \text{ m}^{-3}$, $T_0 = 5000 \text{ K}$, $m = 4.65 \times 10^{-26} \text{ kg}$, the molecular diameter is $d = 4.11 \times 10^{-10} \text{ m}$, the viscosity index is $\omega = 0.74$, the angular scattering parameter is $\alpha = 1.36$, and the Schmidt number is $Sc = 1/1.34$ (Bird 1994). Initially, simulation particles with positive velocity in the x_1 direction follow the equilibrium distribution at 4500 K, while those moving in the opposite direction follow the equilibrium distribution at 5500 K, see figure 1a and 1b, so that initial heat fluxes in all DoF are generated. Then the evolution of heat flux is monitored until the entire system reaches thermal equilibrium, see figure 1c. Ensemble averaged is taken from 3000 independent runs to get the time derivative of heat flux in figure 1d. Finally, the following relaxation rates are

extracted by solving the linear regression problem (2.21) with the least squares method:

$$\begin{bmatrix} A_{tt} & A_{tr} & A_{tv} \\ A_{rt} & A_{rr} & A_{rv} \\ A_{vt} & A_{vr} & A_{vv} \end{bmatrix} = \begin{bmatrix} 0.786 & -0.208 & 0.003 \\ -0.047 & 0.883 & -0.049 \\ -0.004 & -0.038 & 0.772 \end{bmatrix}. \quad (4.2)$$

Hence, according to (2.29), we have $f_t = 2.3635$, $f_r = 1.3979$, $f_v = 1.3825$, and $f_{eu} = 1.807$. With these parameters, our kinetic model is uniquely determined.

4.2. Fourier flow

The heat transfer in the nitrogen gas between two parallel plates located at $x_2 = 0$ and L_0 are considered, where the temperature of the lower and upper plates are $T_l = 0.8T_0$ and $T_u = 1.2T_0$, respectively. The averaged number density of nitrogen is set to be n_0 , and the characteristic length L_0 is chosen to be the distance between two plates. The Knudsen numbers considered are $\text{Kn} = 0.1$ and 1 . The diffuse boundary conditions are adopted, so that the reflected distributions are

$$\begin{aligned} x_2 = 0, v_2 \geq 0: \quad f_0 &= \frac{n_{in}(x_2 = 0)}{n_0} E_t(T_l), \quad f_1 = \frac{d_r}{2} k_B T_l f_0, \quad f_2 = \frac{d_v}{2} k_B T_l f_0, \\ x_2 = L_0, v_2 \leq 0: \quad f_0 &= \frac{n_{in}(x_2 = L_0)}{n_0} E_t(T_u), \quad f_1 = \frac{d_r}{2} k_B T_u f_0, \quad f_2 = \frac{d_v}{2} k_B T_u f_0, \end{aligned} \quad (4.3)$$

where n_{in} is determined by the flux of incident number density of gas at the plates:

$$\begin{aligned} n_{in}(x_2 = 0) &= - \left(\frac{2m\pi}{k_B T_l} \right)^{1/2} \int_{v_2 < 0} v_2 f_0 d\mathbf{v}, \\ n_{in}(x_2 = L_0) &= \left(\frac{2m\pi}{k_B T_u} \right)^{1/2} \int_{v_2 > 0} v_2 f_0 d\mathbf{v}. \end{aligned} \quad (4.4)$$

Numerical results from the kinetic model (3.7) and DSMC are shown in figure 2. For both $\text{Kn} = 0.1$ and $\text{Kn} = 1$, excellent agreement in the density and temperature are observed, where the maximum relative error in the translational heat flux is less than 3%. Meanwhile, profiles of translational, rotational and vibrational temperatures nearly overlap, although the relaxation times for different DoF are different. Additionally, the rotational and vibrational heat flux are almost the same (figure 2f), due to the close values of the rotational and vibrational thermal conductivities. Thus, it is clearly seen that the values of collision number Z_r and Z_v do not have influence on the distribution of macroscopic quantities for the steady-state planar Fourier flow.

We define an effective thermal conductivity of the system by

$$\kappa_e = -q \frac{L_0}{\Delta T}. \quad (4.5)$$

With the increase of Knudsen number, κ_e decreases due to the wall confinement that effectively increases the thermal resistance. For instances, the ratio between the translational and rotational/vibrational thermal conductivities in the continuum limit is around $\kappa_t/\kappa_{r,v} = 2.55$, which decreases to 2.42 and 2.21 when $\text{Kn} = 0.1$ and $\text{Kn} = 1$, respectively.

4.3. Couette flow

The configuration of the Couette flow is the same as the Fourier flow, while the temperature of both plates are kept the same at T_0 , and the velocity of lower and upper plates are $v_1 = -v_m$ and $v_1 = v_m$, respectively. Due to the symmetry, only half of the domain ($L_0/2 \leq x_2 \leq L_0$) is simulated. The diffuse boundary condition at $x_2 = L_0$ yields:

$$v_2 \leq 0: \quad f_0 = \frac{n_{in}(x_2 = L_0)}{n_0} E_t(T_u), \quad f_1 = \frac{d_r}{2} k_B T_0 f_0, \quad f_2 = \frac{d_v}{2} k_B T_0 f_0, \quad (4.6)$$

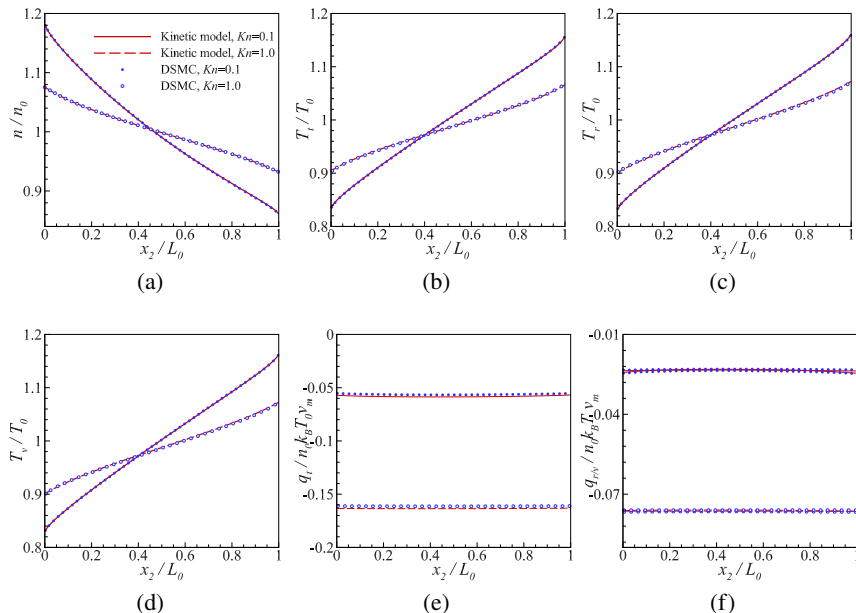


Figure 2: Comparisons of the (a) density, (b) translational temperature, (c) rotational temperature, (d) vibrational temperature, (e) translational heat flux and (f) rotational/vibrational heat flux of nitrogen between our kinetic model (lines) and DSMC (circles) for the Fourier flows.

where $n_{in}(x_2 = L_0)$ is determined as the same way as (4.4), while the symmetrical condition at $x_2 = L_0/2$ reads

$$v_2 \geq 0: \quad f_0 = f_0(-v_1, -v_2, v_3), \quad f_1 = \frac{d_r}{2} k_B T f_0, \quad f_2 = \frac{d_v}{2} k_B T f_0, \quad (4.7)$$

The results from our kinetic model and the DSMC simulation at $\text{Kn} = 0.5$ are shown in figure 3, which demonstrates the accuracy of our model. The vibrational temperature is much lower than the rotational one, since in this problem the energy increase in internal DoF only comes from the exchange with translational ones. Thus, larger collision number leads to less increase in internal temperature at the same distance from the wall (due to the infrequent relaxation with the translational mode), and also contributes less to the heat flux.

4.4. Creep flow driven by the Maxwell demon

The creep flow driven by the Maxwell demon is a thought test (Li et al. 2021), where each gas molecule is subjected to an external acceleration based on its kinetic energy:

$$a_1 = a_0 \left(\frac{v_1^2}{v_m^2} - \frac{3}{2} \right). \quad (4.8)$$

That is, fast molecules are forced towards the positive direction, while the slow molecules move in opposite direction.

Consider the nitrogen flow driven by the Maxwell demon confined between two parallel plates with distance L_0 apart. To solve the force-driven flow, we choose small values of a_0 so that the gas flow deviates only slightly from the global equilibrium; the acceleration acting on the molecules

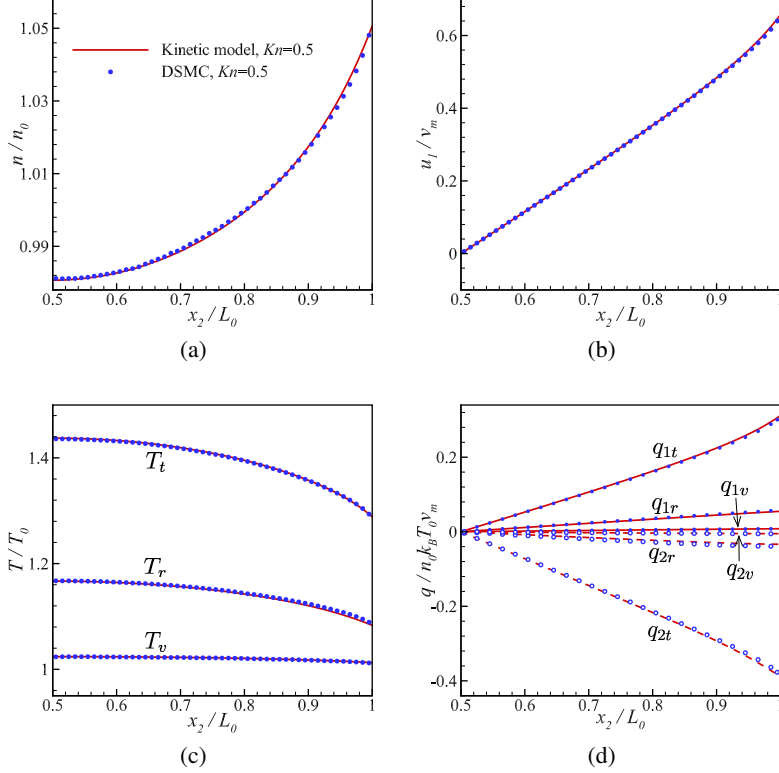


Figure 3: Comparisons of the (a) density, (b) flow velocity, (c) temperature and (d) heat flux q_1 in the flow direction and q_2 perpendicular to flow direction of nitrogen, between our kinetic model (red lines) and DSMC simulations (blue circles) for the one-dimensional Couette flow at $Kn = 0.5$.

is linearised, which results in the source terms at right-hand side of model equations (3.7):

$$\begin{aligned}
 \frac{\partial f_0}{\partial t} + \mathbf{v} \cdot \frac{\partial f_0}{\partial \mathbf{x}} &= Q(f_0) + \frac{g_{0r} - g_{0t}}{Z_r \tau} + \frac{g_{0v} - g_{0t}}{Z_v \tau} - \frac{2a_0 L_0}{v_m^2} v_1 E_t(T_0) \left(\frac{v_1^2}{v_m^2} - \frac{5}{2} \right), \\
 \frac{\partial f_1}{\partial t} + \mathbf{v} \cdot \frac{\partial f_1}{\partial \mathbf{x}} &= \frac{g'_{1t} - f_1}{\tau} + \frac{g_{1r} - g_{1t}}{Z_r \tau} + \frac{g_{1v} - g_{1t}}{Z_v \tau} - \frac{d_r a_0 L_0}{v_m^2} v_1 k_B T_0 E_t(T_0) \left(\frac{v_1^2}{v_m^2} - \frac{5}{2} \right), \\
 \frac{\partial f_2}{\partial t} + \mathbf{v} \cdot \frac{\partial f_2}{\partial \mathbf{x}} &= \frac{g'_{2t} - f_2}{\tau} + \frac{g_{2r} - g_{2t}}{Z_r \tau} + \frac{g_{2v} - g_{2t}}{Z_v \tau} - \frac{d_v a_0 L_0}{v_m^2} v_1 k_B T_0 E_t(T_0) \left(\frac{v_1^2}{v_m^2} - \frac{5}{2} \right). \quad (4.9)
 \end{aligned}$$

The plates at rest are fully diffuse, then the boundary conditions are simply given by (4.3) and (4.4), but with the wall temperature replaced by T_0 .

Figure 4 shows the good agreement between the solution of our kinetic model and DSMC at $Kn = 1$. The rotational/vibrational heat flux is one/two order of magnitude smaller than the translational heat flux, which shows negligible contribution to the total heat transfer in this problem.

To assess the influence of the thermal relaxation rates on the creep flow, two more cases are conducted by varying the values of the matrix A but keeping the Eucken factors fixed. More

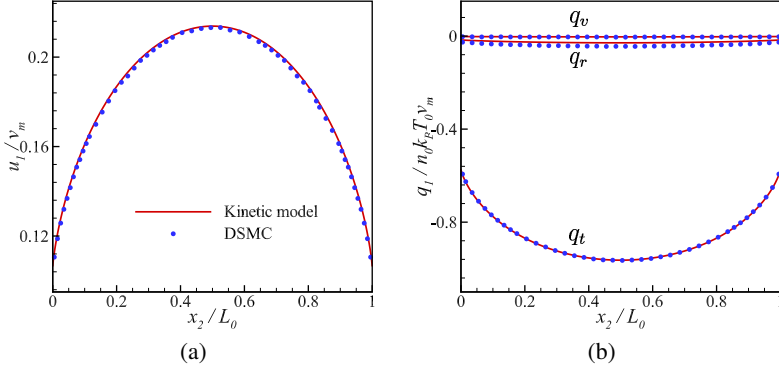


Figure 4: Comparisons of the (a) velocity and (b) heat flux in flow direction of nitrogen between kinetic model (lines) and DSMC simulations (circles) for one-dimensional creep flow driven by the Maxwell demon at $\text{Kn} = 1$. Both the flow velocity and the heat flux have been further normalized by $2a_0L_0/v_m^2$.

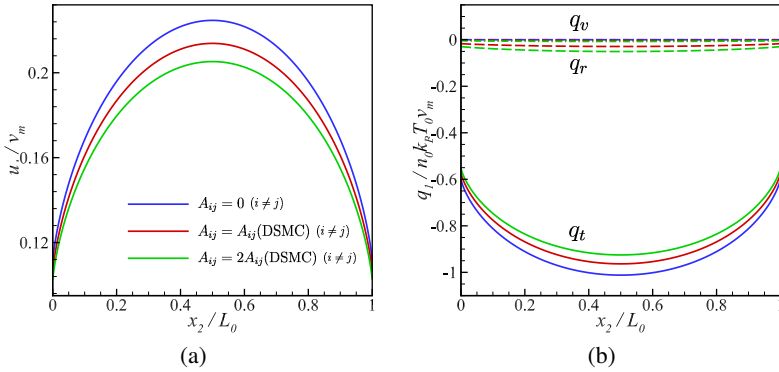


Figure 5: Same as figure 4, except that the off-diagonal elements in A are set to be zero (blue), the values from DSMC (red) and double of those from DSMC (green), respectively.

specifically, the off-diagonal elements in A in the two cases are set to be zero and double of those given by DSMC, respectively. The values of diagonal elements are calculated based on (2.29) using the fixed Eucken factors. Figure 5 shows that these relaxation rates affect the flow velocity and heat fluxes, despite that the thermal conductivities are fixed. In particular, when the off-diagonal elements in A are zero, the heat fluxes of different types of DoF are decoupled, so that the internal heat fluxes are exactly zero. This situations occur in many traditional kinetic models, such as the Rykov model and the ellipsoidal-statistical BGK model. This example demonstrates the importance of recovering the fundamental thermal relaxation process rather than the apparent thermal conductivities in rarefied gas flow simulations.

4.5. Normal shock wave

In the simulations of normal shock wave of nitrogen, the upstream number density $n_u = n_0 = 2.69 \times 10^{25} \text{m}^{-3}$ and temperature $T_u = T_0 = 3993.8 \text{K}$ are chosen to be the reference values, which also determine the characteristic length to be $L_0 = 16\mu(T_0)/(5n_0\sqrt{2\pi mk_B T_0})$ and hence $\text{Kn} = 5\pi/16$ in this problem. The total length of the simulation domain is $90L_0$, so that the

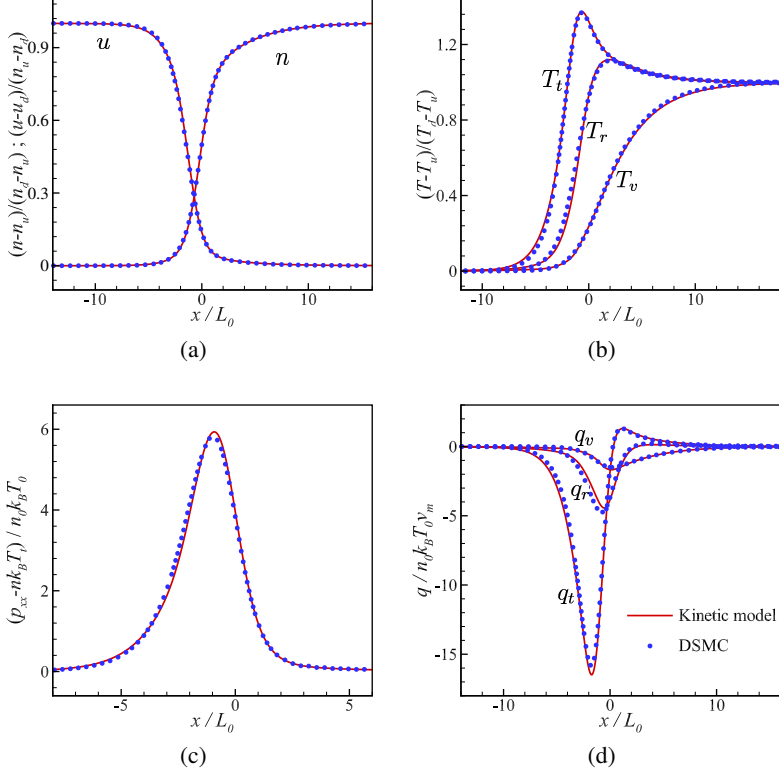


Figure 6: Comparisons of the (a) density and velocity, (b) temperature, (c) deviated pressure and (d) heat flux of nitrogen between our kinetic model (lines) and DSMC (circles) for normal shock wave at Ma = 5.

boundary conditions at both ends can be approximated by equilibrium states (the wave front is initially located at $x = 0$):

$$\begin{aligned}
 x = -30L_0, v \geq 0 : \quad & f_0 = \frac{n_u}{n_0} E_t(T_u), \quad f_1 = \frac{d_r}{2} k_B T_u f_0, \quad f_2 = \frac{d_v}{2} k_B T_u f_0, \\
 x = 60L_0, v \leq 0 : \quad & f_0 = \frac{n_d}{n_0} E_t(T_d), \quad f_1 = \frac{d_r}{2} k_B T_d f_0, \quad f_2 = \frac{d_v}{2} k_B T_d f_0,
 \end{aligned} \quad (4.10)$$

where the subscripts u, d represent the upstream and downstream end, respectively. Given the Mach number, macroscopic quantities at the downstream end are determined by the Rankine–Hugoniot relation.

Numerical results of both the kinetic model (3.7) and DSMC are compared in figure 6, when the Mach number is Ma = 5. As expected, the model equations reproduce the structure of normal shock wave with high accuracy. The rotational and vibrational collision numbers, Z_r and Z_v , which affect energy exchange rate between internal and translational modes, play roles in the difference of rotational and vibrational temperatures. That is, the distance for vibrational temperature to reach equilibrium are much longer than that for rotational modes. This is consistent with the fact that we set $Z_v = 10Z_r$.

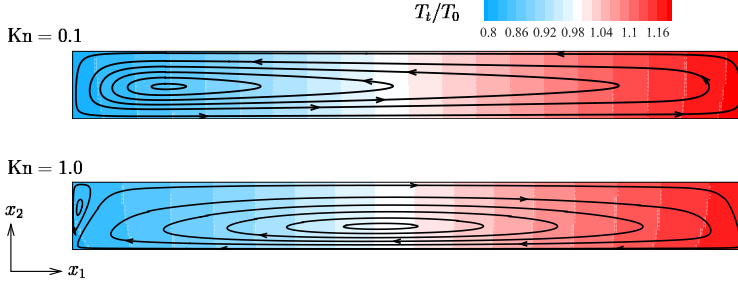


Figure 7: The flow field of thermal transpiration of nitrogen in the cavity solved by kinetic model equations at $\text{Kn} = 0.1$ and 1 , and viscosity index $\omega = 0.74$.

5. Application to two-dimensional thermally induced microflow

Have validated the kinetic model (3.7), we investigate the thermal transpiration of molecular gas in a cavity and the Knudsen force on a micro-beam. The viscosity index is varied to examine the effect of intermolecular potential on thermally induced flows. The deterministic numerical method is suited in this case since the flow speed is usually very small.

5.1. Thermal transpiration in cavity

Consider a two-dimensional rectangular cavity with aspect ratio of 5, and the length of the short side is set to be the characteristic length L_0 . The temperature of the two ends are maintained at $T_w(x_1 = 0) = 0.8T_0$ and $T_w(x_1 = 5L_0) = 1.2T_0$, respectively, and that of the side walls are linearly distributed from $0.8T_0$ to $1.2T_0$. Only the lower half of the cavity ($0 \leq x_1 \leq 5L_0$, $0 \leq x_2 \leq L_0/2$) is simulated owing to the symmetry, and all walls scatter gas molecules diffusely, so that the boundary conditions at the solid walls are

$$f_0 = \frac{n_{in}(x_1)}{n_0} E_t(T_w(x_1)), \quad f_1 = \frac{d_r}{2} k_B T_w(x_1) f_0, \quad f_2 = \frac{d_v}{2} k_B T_w(x_1) f_0, \quad (5.1)$$

while that at the symmetry line ($x_2 = L_0/2, v_2 \leq 0$) is

$$f_0 = f_0(v_1, -v_2, v_3), \quad f_1 = \frac{d_r}{2} k_B T f_0, \quad f_2 = \frac{d_v}{2} k_B T f_0, \quad (5.2)$$

where $n_{in}(x_1)$ is determined similar to (4.4).

5.1.1. Flow field and its mechanism

The flow field is show in figure 7, when $\text{Kn} = 0.1$ and 1 . A large vortex occupies almost the entire simulation domain, which is formed by two competing mechanisms. The diffuse wall generates a steady thermal transpiration, which pushes the gas from the cold end to the hot end. As a result, gas molecules accumulate at the hot end and increase the pressure there, which induces the Poiseuille flow from the hot end to the cold end. Consequently, the thermal transpiration and the Poiseuille flow that are in the opposite directions form the entire vortex. Since in the steady state the horizontal mass flow rate along any vertical line is zero, the rotational direction of the vortex depends on the relative strength of the thermal transpiration and Poiseuille flow. For example, when the Knudsen number is small, the parabolic velocity profile of the Poiseuille flow between two parallel plates is rather steep (the velocity at the channel centre is much larger than that near the solid wall), while that of thermal is very flat. Therefore, the major vortex rotates anticlockwise. On the contrary, when the Knudsen number is large, the velocity profile in thermal transpiration is steeper than that in the Poiseuille flow, so the major vortex rotates clockwise.

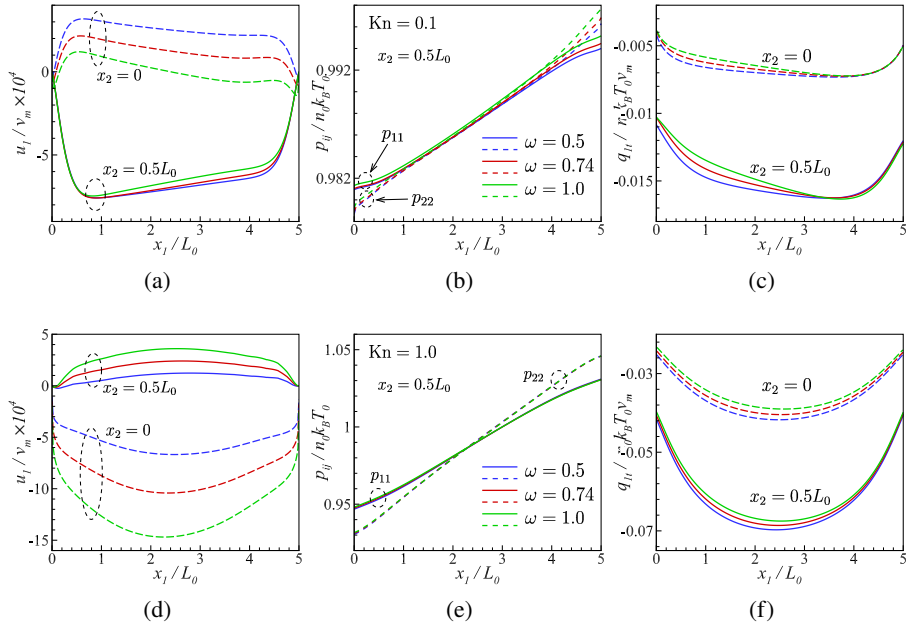


Figure 8: The thermal transpiration of nitrogen in a cavity. The viscosity index is $\omega = 0.5$ (blue), 0.74 (red) and 1.0 (green). (a, d) velocity in x_1 direction, (b, e) normal pressure p_{11} and p_{22} , (c, f) translational heat flux in x_1 direction. Macroscopic quantities are plotted along the central line $x_2 = 0.5L_0$ (solid lines) and the wall $x_2 = 0$ (dashed lines). The Knudsen number is $\text{Kn} = 0.1$ and 1 in the first and second rows, respectively.

5.1.2. Influence of intermolecular potential

The influence of the intermolecular potential is investigated by varying the viscosity index ω , while fixing the relaxation rates and all transport coefficients at the reference temperature. The values of viscosity index are chosen to represent the hard sphere molecules ($\omega = 0.5$), the nitrogen molecules ($\omega = 0.74$) and Maxwell molecules ($\omega = 1$). Figure 8 compares the horizontal velocity, normal pressure and translational heat flux distribution with different ω , when $\text{Kn} = 0.1$ and 1 . Clearly, the most significant impact of the intermolecular potential is the change of the flow velocity. When $\text{Kn} = 0.1$, the slip velocity on the wall ($x_2 = 0$) varies dramatically with ω , while that along the central line ($x_2 = 0.5L_0$) does not change that much. When $\text{Kn} = 1$, significant variation of the flow velocity occurs over the entire domain, and the maximum speed located at the wall increases by 2.2 times, when ω is changed from 0.5 to 1 .

The pressure difference generated at the two ends of the cavity is shown in figure 8b and 8e. It is seen that, the change in normal pressure in both x_1 and x_2 directions is slight at $\text{Kn} = 0.1$, and even negligible at $\text{Kn} = 1$. Besides, the variation of translational heat flux is also not that significant. In general, the heat flux in the low temperature region decreases with the increase of ω , since the effective shear viscosity and hence the thermal conductivity is lower in this region based on (3.10). The situation in the high temperature region is reversed, i.e., the heat flux increases with ω . Since the temperature varies from $0.8T_0$ to $1.2T_0$ in the system, the difference in viscosity and thermal conductivity does not exceed 10% when ω changing from 0.5 to 1 , and thus the difference in heat flux is also within this range.

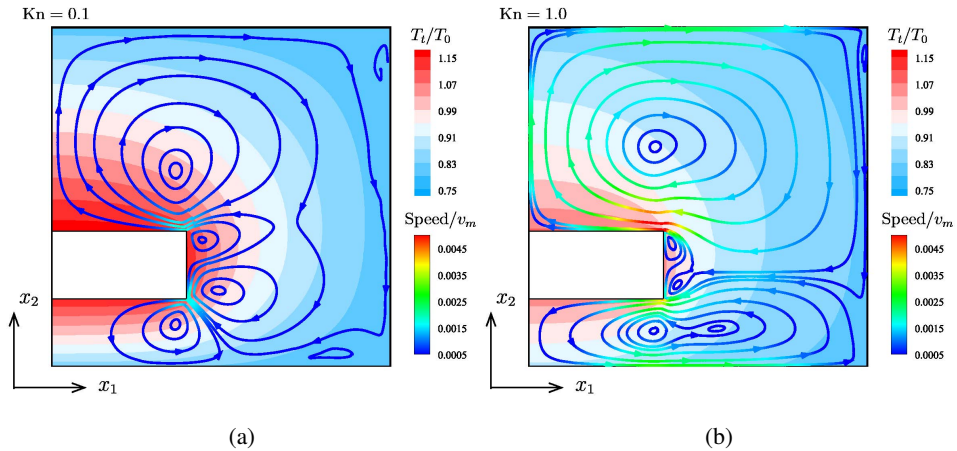


Figure 9: Flow field of nitrogen surrounding the heated micro-beam in cavity, which is solved by the kinetic model (3.7) when (a) $\text{Kn} = 0.1$ and (b) $\text{Kn} = 1$, and viscosity index $\omega = 0.74$. The background contour is the distribution of translational temperature.

5.2. Knudsen force on micro-beam

The Knudsen force acting on a heated micro-beam adjacent to a cold substrate is a mechanical force created by the surrounding thermally nonequilibrium rarefied gas. As one type of the thermal forces, which emerges mainly in micro/nano devices with integrated heaters due to the advent of microfabrication techniques nowadays, the Knudsen force has been investigated numerically and experimentally (Passian et al. 2003; Li et al. 2013; Pikus et al. 2019). Both the magnitude and direction of the force is important, since it may significantly affect the performance of many micro/nano devices, say, the accuracy of atomic force microscopy (Passiana et al. 2003). The Knudsen force induced by molecular gas has not been systematically studied, especially the underlying mechanism and the influence of intermolecular potential.

The system considered here is a heated micro-beam ($L_0 \times 2L_0$) placed inside a cold chamber ($5L_0 \times 10L_0$), and the centre of the micro-beam shift towards negative x_2 direction by a distance L_0 with respect to the centre of the chamber. The temperature of the micro-beam and chamber are maintained at $1.2T_0$ and $0.8T_0$, respectively, and all the surface are fully diffuse. Due to the symmetry, only the right half of the system ($0 \leq x_1 \leq 5L_0$, $0 \leq x_2 \leq 5L_0$) is simulated.

The implicit discontinuous Galerkin (DG) method is employed in the numerical simulations (Su et al. 2020), and the fourth-order approximating polynomials are used in the DG scheme. The computational domain is partitioned by unstructured triangles with refinement in the vicinity of the beam surfaces. To be specific, the total number of elements is 1790 when $\text{Kn} = 0.1$ and 1738 when $\text{Kn} = 1$. The molecular velocity space is truncated by $[-7v_m, 7v_m]^3$, and 64 non-uniform velocity points are used to discretize v_1 and v_2 , while 32 uniform points are used for v_3 . And in the velocity space the fast spectral method is incorporated into the DG discretization to evaluate the collision operator, where $32 \times 32 \times 32$ equidistant frequencies are employed.

5.2.1. Flow field and its mechanism

The translational temperature contour and flow field are shown in figure 9. The flow structures are similar for the two cases at $\text{Kn} = 0.1$ and 1, although the relative strength varies significantly. The temperature of gas changes rapidly around the sharp corners, and forms large temperature gradient normal to the surface of the micro-beam. In analogy to the asymptotic analysis of

Boltzmann equation for monatomic gas (Sone 2002), three types of thermally induced flow exist around the micro-beam in the molecular gas, namely, the thermal stress slip flow, the nonlinear thermal stress flows, and the thermal edge flow. The first two are caused by the normal temperature gradient along the wall, and the flow speed reaches the maximum values at the sharp corners. However, they are in the direction opposite to that shown in figure 9. On the contrary, the mechanism of the thermal edge flow is similar to that of the thermal transpiration, and the flow is in the same direction as that observed in figure 9. The thermal edge flow is fairly strong within a wide range of Knudsen number, especially becomes strongest in the transition regime. As demonstrated in figure 9, the flow speed is much larger when $\text{Kn} = 1$ than that when $\text{Kn} = 0.1$.

Figure 10b shows the magnitude of heat flux along the surfaces of the heated micro-beam at $\text{Kn} = 1$, where the result of nitrogen gas ($\omega = 0.74$) is indicated by red line. And its direction is normal to the surface, due to the isothermal walls. The strongest heat flux occurs at the corners of the micro-beam, where the normal temperature gradient is largest. Despite the different collision numbers of rotational and vibrational modes, the rotational and vibrational heat fluxes are almost the same. Meanwhile, it is found that the total internal heat flux is approximately equal to the translational one. Therefore, although the relaxation time of internal relaxation is usually much longer than that of the translational mode, the heat fluxes carried by rotational and vibrational modes could be considerable. In particular, when a gas molecule consists of more atoms, it could have more number of internal DoF and thus contributes more to the total heat flux.

5.2.2. The Knudsen force on the micro-beam

The thermally induced flows redistribute the gas molecules and hence the pressure in the chamber. Therefore, it is expected to have a net force acting on the beam. The resultant force in horizontal direction is zero due to the symmetry about $x_1 = 0$. To investigate the vertical force acting on the beam, the normal pressure p_{22} on the top and bottom surfaces and shear stress p_{12} along the right surface of the beam are shown in figure 10c. The variation of normal pressure is found to be small along the surfaces, which is around 1%. Therefore, although the normal pressure p_{22} is about two orders of magnitude larger than the shear stress p_{12} , the resultant force of the normal pressure F_n is of the same order or even smaller than the resultant shear force F_s . This is consistent with the fact that the origin of the Knudsen force is the thermally induced flows, which determine the order of magnitude of the shear force. Thus, the Knudsen force should be sensitive to the shear force. When $\text{Kn} = 0.1$, $F_n = 3.52 \times 10^{-4} n_0 k_B T_0 L_0$ is much smaller than $F_s = 1.32 \times 10^{-3} n_0 k_B T_0 L_0$, and then the beam is subjected to a total Knudsen force $F = 1.67 \times 10^{-3} n_0 k_B T_0 L_0$ pointing to the positive x_2 direction. When $\text{Kn} = 1$, the magnitudes of both F_n and F_s are larger than those when $\text{Kn} = 0.1$ but in opposite directions. Competed by these two forces, the total force is $F = 5.06 \times 10^{-4} n_0 k_B T_0 L_0$, which points to the positive x_2 direction but is relatively small in its magnitude.

5.2.3. Influence of intermolecular potential

The effect of intermolecular potential reflected in the viscosity index ω is also investigated. Similar to that in the thermal transpiration, the thermally induced velocity around the micro-beam changes significantly with ω as shown in figure 10a. For instance, when $\text{Kn} = 1$, the maximum magnitude of velocity at the corner is increased by 1.74 times when ω changes from 0.5 to 1. However, figures 10b and 10c show that the heat flux and stress are not affected that much: the maximum difference is around 3.8% in heat flux and less than 0.5% in normal pressure.

Both the magnitude and orientation of the resultant force acting on the micro-beam is found to be very sensitive to the viscosity index. Table 1 lists the normal, shear and total force for different ω . As ω increases, the normal force tends to be stronger in negative x_2 direction. However, the shear force acting on the side surfaces increases slightly in the positive x_2 direction. When $\text{Kn} = 1$, the opposite trends reverse the direction of the total force. It also implies that a zero net force

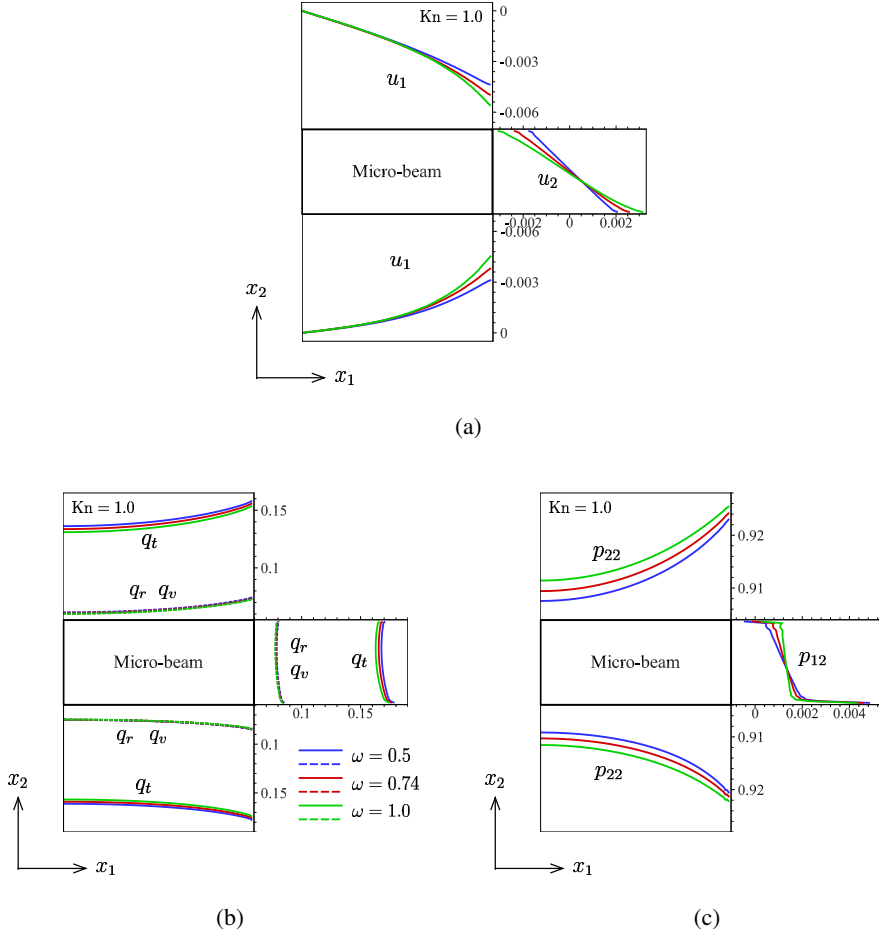


Figure 10: The distribution of (a) velocity (normalized by v_m), (b) heat flux (normalized by $n_0 k_B T_0 v_m$) and (c) normal stress p_{22} and shear stress p_{12} (normalized by $n_0 k_B T_0$) along the surface of the heated micro-beam solved by kinetic model equations when $Kn = 1$. The viscosity index $\omega = 0.5, 0.74, 1$ are represented by blue, red and green lines, respectively.

exist at certain value of ω , which happens to be around 0.74 (the value for variable soft sphere model of nitrogen) in this configuration.

6. Conclusions

A kinetic model for molecular gas with internal DoF has been proposed. Compared with the previous works on the model equations, there are two features in our kinetic model: (i) realization of molecular velocity-dependent collision time, and consistent with the Boltzmann equation for monatomic gas when the translational-internal energy exchange is extremely slow; (ii) recovery of thermal relaxation processes and rates, and all transport coefficients. Thus, this kinetic model has the ability to describe the influence of intermolecular potentials.

The accuracy of our model has been demonstrated by comparing with DSMC simulations for one-dimensional Fourier flow, Couette flow, creep flow driven by the Maxwell demon and normal shock wave. Then, the thermal transpiration and Knudsen force acting on micro-beam,

Kn	ω	$F_n \times 10^3$ ($n_0 k_B T_0 L_0$)	$F_s \times 10^3$ ($n_0 k_B T_0 L_0$)	$F \times 10^3$ ($n_0 k_B T_0 L_0$)
0.1	0.5	0.646	1.29	1.93
	0.74	0.352	1.32	1.67
	1	0.222	1.38	1.60
1	0.5	0.274	2.63	2.91
	0.74	-2.22	2.73	0.506
	1	-4.70	2.80	-1.90

Table 1: The Knudsen force calculated from kinetic model equation (3.7) for the viscosity index $\omega = 0.5, 0.74$, and 1. F_n is the resultant normal force from top and bottom surfaces of the beam, F_s is the resultant shear force from the side surfaces, and the total force $F = F_n + F_s$, where the positive value indicates that the force points to the positive x_2 direction.

which would need extreme long simulation time in DSMC, are investigated. It is found that the intermolecular potential, reflected through the viscosity index, has a big impact on the flow velocity and the Knudsen force exerted on the beam. This discovery is useful in the design of micro-electromechanical systems for microstructure actuation and gas sensing (Strongrich & Alexeenko 2015; Strongrich et al. 2017).

With the multiscale numerical method (Su et al. 2019b; Zhu et al. 2021) which is able to find the steady-state solution within dozens of iterations, the present kinetic model is expected to find applications in various areas with rarefied molecular gas dynamics, especially for high-temperature problems, such as shock wave that needs accurate velocity-dependent collision time in the kinetic model, as well as for micro flows, where the deterministic numerical method is needed to resolve the small signals.

Declaration of interests

The authors report no conflict of interest.

REFERENCES

- ANDERSON, J. D. 2019 Hypersonic and high temperature gas dynamics. AIAA.
- ANDRIES, PIERRE, LE TALLEC, PATRICK, PERLAT, JEAN-PHILIPPE & PERTHAME, BENOIT 2000a The Gaussian-BGK model of Boltzmann equation with small Prandtl number. *European Journal of Mechanics-B/Fluids* **19** (6), 813–830.
- ANDRIES, P., TALLEC, P. LE, PERLAT, J. & PERTHAME, B. 2000b The Gaussian-BGK model of Boltzmann equation with small Prandtl number. *Eur. J. Mech. B Fluids* **19**, 813–830.
- AOKI, K., BISI, M., GROPPI, M. & KOSUGE, S. 2020 Two-temperature Navier-Stokes equations for a polyatomic gas derived from kinetic theory. *Phys Rev E* **102** (2), 023104.
- BERNARD, F., IOLLO, A. & PUPPO, G. 2019 BGK polyatomic model for rarefied flows. *Journal of Scientific Computing* **78** (3), 1893–1916.
- BHATNAGAR, P. L., GROSS, E. P. & KROOK, M. 1954 A model for collision processes in gases. I. Small amplitude processes in charged and neutral one-component systems. *Phys. Rev.* **94**, 511–525.
- BIRD, G. A. 1994 Molecular Gas Dynamics and the Direct Simulation of Gas Flows. Oxford University Press Inc, New York: Oxford Science Publications.
- BORGNACKE, C. & LARSEN, P. S. 1975 Statistical collision model for Monte Carlo simulation of polyatomic gas mixture. *Journal of Computational Physics* **18** (4), 405–420.

- BRUNO, D. & GIOVANGIGLI, V. 2011 Relaxation of internal temperature and volume viscosity. *Physics of Fluids* **23**, 093104.
- CHAPMAN, S. & COWLING, T. G. 1970 The Mathematical Theory of Non-uniform Gases. Cambridge University Press.
- COLONNA, G., ARMENISE, I., BRUNO, D. & CAPITELLI, M. 2006 Reduction of state-to-state kinetics to macroscopic models in hypersonic flows. *Journal of Thermophysics and Heat Transfer* **20** (3), 477–486.
- DAUVOIS, Y., MATHIAUD, J. & MIEUSSENS, L. 2020 An ES-BGK model for vibrational polyatomic gases. *arXiv preprint arXiv:2007.02727*.
- EUCKEN, A. 1913 Über das Wärmeleitvermögen, die spezifische Wärme und die innere Reibung der Gase. *Phys. Z* **14**, 324.
- FREZZOTTI, A. 2007 A numerical investigation of the steady evaporation of a polyatomic gas. *European Journal of Mechanics-B/Fluids* **96** (1), 93–104.
- GIMELSHEIN, N. E., GIMELSHEIN, S. F. & LAVIN, D. A. 2002 Vibrational relaxation rates in the direct simulation Monte Carlo method. *Phys. Fluids* **14**, 4452.
- GORJI, M. H. & JENNY, P. 2013 A Fokker-Planck based kinetic model for diatomic rarefied gas flows. *Phys. Fluids* **25**, 062002.
- HAAS, B. L., HASH, D. B., BIRD, G. A., LUMPKIN III, F. E. & HASSAN, H. A. 1994 Rates of thermal relaxation in direct simulation Monte Carlo methods. *Phys. Fluids* **6**, 2191.
- HADJICONSTANTINOY, N. G., GARCIA, A. L., BAZANT, M. Z. & HE, G. 2003 Statistical error in particle simulations of hydrodynamic phenomena. *J. Comput. Phys.* **187** (1), 274–297.
- HOLWAY, L. H. 1966 New statistical models for kinetic theory: methods of construction. *Phys. Fluids* **9**, 1658–1673.
- HOLWAY JR, LOWELL H 1966 New statistical models for kinetic theory: methods of construction. *The physics of fluids* **9** (9), 1658–1673.
- IVANO, M. S. & GIMELSHEIN, SF. 1998 Computational hypersonic rarefied flows. *Annual Review of Fluid Mechanics* **30**, 469–505.
- KARNIADAKIS, G., BESKOK, A. & ALURU, N. R. 2005 Microflows and Manoflows: Fundamentals and Simulations. Springer, New York.
- KLINGENBERG, C., PIRNER, M. & PUPPO, G. 2018 A consistent kinetic model for a two-component mixture of polyatomic molecules. *arXiv preprint arXiv:1806.11486*.
- LI, Q., LIANG, T. & YE, W. 2013 Shape-dependent orientation of thermophoretic forces in microsystems. *Physical Review E* **88** (23), 033020.
- LI, Q., ZENG, J., SU, W. & WU, L. 2021 Uncertainty quantification in rarefied dynamics of molecular gas: rate effect of thermal relaxation. *J. Fluid Mech.* **917**, A58.
- LOYALKA, S. K. 1990 Slip and jump coefficients for rarefied gas flows: variational results for Lennard-Jones and $n(r)-6$ potentials. *Physica A: Statistical Mechanics and its Applications* **163** (3), 813–821.
- LOYALKA, S. K. & STORVICK, T. S. 1979 Kinetic theory of thermal transpiration and mechanocaloric effect. iii. flow of a polyatomic gas between parallel plates. *J. Chem. Phys.* **71**, 339–350.
- MALIK, M. R. & ANDERSON, E. C. 1991 Real gas effects on hypersonic boundary-layer stability. *Physics of Fluids A: Fluid Dynamics* **3** (5), 803–821.
- MASON, E. A. 1963 Molecular relaxation times from thermal transpiration measurements. *J. Chem. Phys.* **39**, 522–526.
- MASON, E. A. & MONCHICK, L. 1962 Heat conductivity of polyatomic and polar gases. *J. Chem. Phys.* **36**, 1622.
- MATHIAUD, J. & MIEUSSENS, L. 2020 BGK and Fokker-Planck models of the Boltzmann equation for gases with discrete levels of vibrational energy. *Journal of Statistical Physics* **178** (5), 1076–1095.
- MORSE, T. F. 1964 Kinetic model for gases with internal degrees of freedom. *Phys. Fluids* **7**, 159–169.
- PASSIAN, A., WARMACK, R. J., FERRELL, T. L. & THUNDAT, T. 2003 Thermal transpiration at the microscale: A crookes cantilever. *Phys. Rev. Lett* **90** (12), 124503.
- PASSIANA, A., WARMACK, R. J., WIGA, A., FARAHIA, R. H., MERIAUDEAUB, F., FERRELLA, T. L. & THUNDATA, T. 2003 Observation of knudsen effect with microcantilevers. *Ultramicroscopy* **97**, 401–406.
- PFEIFFER, M., NIZENKOV, P., MIRZA, A. & FASOULAS, S. 2016 Direct Simulation Monte Carlo modeling of relaxation processes in polyatomic gases. *Physics of Fluids* **28** (2), 027103.
- PIKUS, A., SEBASTIÃO, I. BORGES, STRONGRICH, A. & ALEXEENKO, A. 2019 Characterization of a Knudsen force based vacuum sensor for N_2H_2O gas mixtures. *Vacuum* **161**, 130–137.

- PIRNER, M. 2018 A BGK model for gas mixtures of polyatomic molecules allowing for slow and fast relaxation of the temperatures. *Journal of Statistical Physics* **173** (6), 1660–1687.
- PLIMPTON, S. J., MOORE, S. G., BORNER, A., STAGG, A. K., KOEHLER, T. P., TORCZYNSKI, J. R. & GALLIS, M. A. 2019 Direct Simulation Monte Carlo on petaflop supercomputers and beyond. *Phys. Fluids* **31** (8), 086101.
- PORODNOV, B. T., KULEV, A. N. & TUCHVETOV, F. T. 1978 Thermal transpiration in a circular capillary with a small temperature difference. *J. Fluid Mech.* **88** (4), 609–622.
- RAHIMI, B. & STRUCHTRUP, H. 2016 Macroscopic and kinetic modelling of rarefied polyatomic gases. *Journal of Fluid Mechanics* **806**, 437–505.
- RYKOV, V. 1975 A model kinetic equation for a gas with rotational degrees of freedom. *Fluid Dyn.* **10**, 959–966.
- SHAKHOV, E. M. 1968a Approximate kinetic equations in rarefied gas theory. *Fluid Dynamics* **3**, 112–115.
- SHAKHOV, E. M. 1968b Generalization of the Krook kinetic relaxation equation. *Fluid Dyn.* **3** (5), 95–96.
- SHARIPOV, F. & BERTOLDO, G. 2009 Poiseuille flow and thermal creep based on the Boltzmann equation with the Lennard-Jones potential over a wide range of the Knudsen number. *Phys. Fluids* **21**, 067101.
- SONE, Y. 2002 *Kinetic theory and fluid dynamics*. Birkhauser Boston.
- STRONGRICH, A. & ALEXEENKO, A. 2015 Microstructure actuation and gas sensing by the knudsen thermal force. *Applied Physics Letters* **107** (19), 193508.
- STRONGRICH, A., PIKUS, A., SEBASTIAO, I. B. & ALEXEENKO, A. 2017 Microscale in-plane knudsen radiometric actuator: Design, characterization, and performance modeling. *Journal of Microelectromechanical Systems* **26** (3), 528–538.
- SU, W., WANG, P., LIU, H. H. & WU, L. 2019a Accurate and efficient computation of the Boltzmann equation for Couette flow: Influence of intermolecular potentials on Knudsen layer function and viscous slip coefficient. *J. Comput. Phys.* **378**, 573–590.
- SU, W., WANG, P., ZHANG, Y. & WU, L. 2020 Implicit discontinuous Galerkin method for the Boltzmann equation. *Journal of Scientific Computing* **82** (39).
- SU, W., ZHU, L. H., WANG, P., ZHANG, Y. H. & WU, L. 2019b Can we find steady-state solutions to multiscale rarefied gas flows within dozens of iterations? *arXiv:1906.05280*.
- TAKATA, S. & FUNAGANE, H. 2011 Poiseuille and thermal transpiration flows of a highly rarefied gas: over-concentration in the velocity distribution function. *J. Fluid Mech.* **669**, 242–259.
- TANTOS, C., GHIROLDI, G. P., VALOUGEORGIS, D. & FREZZOTTI, A. 2016 Effect of vibrational degrees of freedom on the heat transfer in polyatomic gases confined between parallel plates. *International Journal of Heat and Mass Transfer* **102**, 162–173.
- TITAREV, V. A. & FROLOVA, A. A. 2018 Application of model kinetic equations to calculations of super- and hypersonic molecular gas flows. *Fluid Dyn.* **53**, 536–551.
- WAGNER, W. 1992 A convergence proof for Bird's direct simulation Monte Carlo method for the Boltzmann equation. *J. Stat. Phys.* **66**, 1011–1044.
- WANG, Z., YAN, H., LI, Q. B. & XU, K. 2017 Unified gas-kinetic scheme for diatomic molecular flow with translational, rotational, and vibrational modes. *J. Comput. Phys.* **350**, 237–259.
- WANG-CHANG, C. S. & UHLENBECK, G. E. 1951 *Transport Phenomena in Polyatomic Gases*. University of Michigan Engineering Research Rept. No. CM-681.
- WU, L., LI, Q., LIU, H. & UBACHS, W. 2020 Extraction of the translational Eucken factor from light scattering by molecular gas. *J. Fluid Mech.* **901**, A23.
- WU, L., LIU, H. H., ZHANG, Y. H. & REESE, J. M. 2015a Influence of intermolecular potentials on rarefied gas flows: Fast spectral solutions of the Boltzmann equation. *Phys. Fluids* **27**, 082002.
- WU, L., REESE, J. M. & ZHANG, Y. H. 2014 Solving the Boltzmann equation by the fast spectral method: application to microflows. *J. Fluid Mech.* **746**, 53–84.
- WU, L., WHITE, C., SCANLON, T. J., REESE, J. M. & ZHANG, Y. H. 2013 Deterministic numerical solutions of the Boltzmann equation using the fast spectral method. *J. Comput. Phys.* **250**, 27–52.
- WU, L., WHITE, C., SCANLON, T. J., REESE, J. M. & ZHANG, Y. H. 2015b A kinetic model of the Boltzmann equation for non-vibrating polyatomic gases. *J. Fluid Mech.* **763**, 24–50.
- ZHU, L. H., PI, X. C., SU, W., LI, Z. H., ZHANG, Y. H. & WU, L. 2021 General synthetic iterative scheme for nonlinear gas kinetic simulation of multi-scale rarefied gas flows. *J. Comput. Phys.* **430**, 110091.